Earthquakes and Structures, *Vol. 8, No. 1 (2014) 101-132*
DOI: http://dx.doi.org/10.12989/eas.2015.8.1.101

Prediction of seismic cracking capacity of glazing systems

William C. O'Brien Jr.[1], Ali M. Memari*[2a] and M.EERI[b]

[1]Architectural Engineer, Wiss, Janney, Elstner Associates, Inc., 10 South LaSalle Street, Suite 2600, Chicago, IL 60603, USA
[2]Hankin Chair in Residential Building Construction, Department of Architectural Engineering, Department of Civil and Environmental Engineering, Penn State University, 219 Sackett Building, University Park, PA 16802, USA

(Received November 5, 2013, Revised May 5, 2014, Accepted May 21, 2014)

Abstract. This research formulates a closed-form equation to predict a glass panel cracking failure drift for several curtain wall and storefront systems. An evaluation of the ASCE 7-10 equation for Dclear, which is the drift corresponding to glass-to-frame contact, shows that the kinematic modeling assumed for formulation of the equation is sound. The equation proposed in this paper builds on the ASCE equation and offers a revision of that equation to predict drift corresponding to cracking failure by considering glazing characteristics such as glass type, glass panel configuration, and system type. The formulation of the proposed equation and corresponding analyses with the ASCE equation is based on compiled experimental data of twenty-two different glass systems configurations tested over the past decade. A final comparative analysis between the ASCE equation and the proposed equation shows that the latter can predict the drift corresponding to glass cracking failure more accurately.

Keywords: curtain wall; drift; glass-to-frame clearance; glass failure; glass panel cracking; prediction; seismic capacity, storefront

1. Introduction

Architectural glass curtain wall systems (Memari 2013) are in widespread use as a favorable way to enclose a building structure in terms of cost effectiveness (WBDG 2009). Additionally, curtain wall systems offer many advantages including vision, natural lighting and energy efficiency over other types of envelope systems (Kim 2011, Richman and Pressnail 2009). As part of the building envelope, glazing systems are important to maintaining the proper function of a building (Lee *et al*. 2002, Gasparella *et al*. 2011). On a taller structure, these can be one of the most expensive systems and cost over 20% of a building's construction budget (NIBS 2008). Past earthquakes such as Northridge in 1994 have exposed the vulnerability of glass curtain wall and storefront systems to significant damage resulting from seismic events (Hamburger 2006). Reconnaissance reports indicate that significant damage can occur to these glass systems, even

*Corresponding author, , Professor Ali Memari, E-mail: memari@engr.psu.edu
[a]Professor, E-mail: obrien2884@gmail.com
[b]Ph.D., E-mail: memari@engr.psu.edu

Copyright © 2015 Techno-Press, Ltd.
http://www.techno-press.org/?journal=eas&subpage=7   ISSN: 2092-7614 (Print), 2092-7622 (Online)

when the primary structural system has sustained little to no damage (EERI 1995). Repair of damaged glass systems can be quite costly to a building owner, and glass breakage that can result in falling glass shards can pose a life-safety hazard to building occupants and pedestrians.

Currently, very few publications are available that can assist design professionals in the proper selection of glazing systems to more effectively resist earthquake damage. Some recent contributions include: Memari 2012, Bull and Cholasky 2012, Eva and Hutchinson 2011, and Hutchinson *et al*. 2011. Equations found in codes such as ASCE 7-10 (2010) primarily give drift limitations on glazing systems. These limitations are based on the glass edge clearances of a system and are aimed at preventing glass fallout, which is a life-safety concern. The goal of this research was to develop a closed-form equation that estimates the cracking capacity of a glass system based on various glazing characteristics in addition to glass-to-frame clearance and glass panel dimensions. The proposed equation can be employed by design professionals to estimate cracking drift.

The current ASCE equation (discussed subsequently) is based on the kinematic response of glass lites held within glazing pockets through rubber gaskets (dry-glazed) subjected to in-plane lateral displacements to predict the drift corresponding to full diagonal corner contact between glass and glazing pocket. In particular, the ASCE equation considers two physical characteristics of a glazing system through the glass-to-frame clearance and dimensions (aspect ratio) of a glass lite. In practical applications, however, satisfaction of the drift criterion is understood as preventing damage to glass.

The accuracy of the ASCE equation is evaluated by comparing the calculated values of drift capacity of different curtain wall configurations with known experimental results. This analysis indicates that the ASCE equation is relatively accurate in predicting glass damages, however, it does not account for different characteristics of glazing systems such as glass type, configuration, glass-to-frame clearance, and aspect ratio that can also affect the capacity. Therefore, a new closed-form equation is presented in this work based on revising the ASCE equation by the addition of factors to account for glazing characteristics such as glass type, configuration, and system type. Additionally, factors are added to refine the effects of sub-standard glass-to-frame clearances and the aspect ratio of the glass panel. Finally, a factor is added for framing-to-structure connections to account for future consideration of this system characteristic. The factors are created from the compiled data from numerous experimental glass studies (Behr *et al*. 1995, Behr 1998, Memari *et al*. 2003, and O'Brien *et al*. 2012). It should be noted that some factors were developed based on a relatively smaller amount of data points than other factors. However, with further research and testing, additional data points can be collected and used to refine the factors and to increase the overall accuracy of the equation. The form of the suggested revised equation, however, need not be affected with additional test data. A subsequent comparison analysis between the developed equation and current ASCE equation is presented.

2. Background

2.1 ASCE and bouwkamp equations

Unlike design for wind loads, currently there are no charts or design aids to help design professionals in the proper selection of glazing systems to more effectively resist earthquake damage. The ASCE 7-10 (ASCE 2010) seismic provisions give an equation for drift limits that glazing systems must meet. Within a larger context, IBC 2006 (ICC 2006) refers to ASCE 7-05 (ASCE 2006) and requires glazing systems to accommodate the building design drift with the intent of addressing life-safety hazards associated with glass fallout. It should be noted that the seismic provisions for glazing systems in ASCE 7-10 are the same as in ASCE 7-05. The provisions require that the following equation be satisfied:

$$\left.\begin{array}{l}\Delta_{\text{fallout}} \geq 1.25 I D_p \\ or \quad\ \geq 0.5\,\text{in.}\end{array}\right\} \text{whichever is greater} \tag{1}$$

where I denotes the importance factor, Δ_{fallout} denotes the drift at which glass fallout from the curtain wall or storefront wall system under consideration is expected to occur, and D_p denotes the drift that the system must be designed to accommodate. D_p is defined as the relative displacement over the height of the glazing component and is a product of the building structural analysis for seismic loads based on ASCE 7-10 with the consideration of displacement amplification factor.

Meeting the ASCE 7-10 provisions as defined by Eq. (1) requires finding the value of Δ_{fallout}. This must be accomplished through an engineering analysis or by the test method prescribed in AAMA 501.6 (AAMA 2009). Since engineering analysis guidelines for glazing systems are not developed to a sufficient degree, the practical way of effectively determining Δ_{fallout} is through mockup testing.

As an alternative to determining Δ_{fallout}, ASCE 7-10 states that the following conditions can be met:

$$D_{clear} \geq 1.25 D_p \tag{2}$$

where D_{clear} is defined as the "relative horizontal (drift) displacement measured over the height of the glass panel under consideration, which causes initial glass-to-frame contact" (ASCE 2010). For rectangular glass panels within a rectangular glazing frame, D_{clear} can be found through the following equation:

$$D_{clear} = 2c_1\left(1 + \frac{h_p c_2}{b_p c_1}\right) \tag{3}$$

where h_p and b_p denote, respectively, the height and width of the rectangular glass panel, c_1 denotes the glass-to-frame clearance between the vertical glass edges and frame member, and c_2 denotes the clearance between the horizontal glass edges and framing member.

The ASCE 7-10 (ASCE 2010) equation has been derived based on the equation presented by Bouwkamp (1961) and Bouwkamp and Meehan (1960), referred to here as the "Bouwkamp Equation". In these studies, the in-plane static behavior of glass panels was studied and experimental variables included the size of the glass panel and configuration type (e.g., monolithic, laminated, or insulting glass unit), panel attachment to the structural frame, the frame material, glass-to-frame clearance, and type of glazing putty. The authors observed that as lateral loading is subjected to the assembly, the glass panel begins to translate horizontally and rotate within the framing while simultaneous framing deformation occurs leading to an initial glass contact with the framing at opposite glass corners. This contact results in glass corner crushing and cracking of the glass panel. Eventually, a diagonal compressive force will also develop that leads to glass panel fallout failure. The authors concluded that the dimensional properties associated with the glass response to lateral loading include glass-to-frame clearances and the height and width of the glass panel (Fig. 1). The Bouwkamp equation that calculates the drift at which a glass panel would be expected to experience cracking and corner crushing is as follows:

$$\Delta - \varphi h = 2c\left(1 + \frac{h}{b}\right) \tag{4}$$

where Δ denotes the total drift between the top and bottom horizontal frame members, φh denotes rotational adjustment considering field framing intersections (equivalent to zero for laboratory conditions), c denotes glass-to-frame clearance, and h and b denote the glass panel height and width, respectively.

The ASCE equation is a slightly revised version of the Bouwkamp equation adopting the physical characteristics of glass-to-frame clearance and glass panel dimensions to model failure capacity, as seen in the comparisons of Eqs. (3) and (4). The ASCE equation also takes into account the differences in glass-to-frame clearance for mullion and transom. The rotational adjustment factor φh is not considered by the ASCE equation. While the ASCE equation is defined as calculating a drift value that corresponds to initial diagonal contact between the glass and framing and is used in the context of preventing glass damage (Behr 1998), it ultimately represents the drift at the point right before a glass panel is expected to experience glass cracking due to seismic induced drift. Accordingly, for this research, it is assumed that the ASCE Eq. (3) represents a drift limit corresponding to glass-to-frame contact experienced before the cracking or crushing of a glass panel occurs,. This drift (D_{clear}) can be regarded as a conservative prediction of the drift corresponding to a cracking failure damage state of glass in the sense that the actual drift at failure is expected to be larger than this drift.

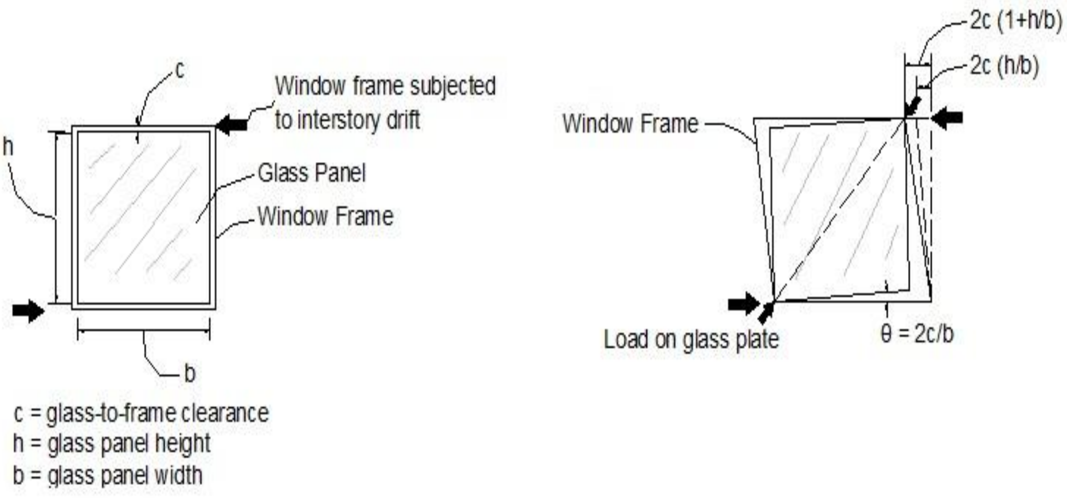

Fig. 1 Glass panel movement under lateral loading and derivation of Bouwkamp equation factors (that the ASCE equation is based on) with depiction of (a) unloaded glass specimen, and (b) loaded glass panel with frame deformation and subsequent glass-to-frame contact at corners of glazing pockets with developed diagonal compressive force (Figure adopted from Sucuoglu and Vallabhan 1997)

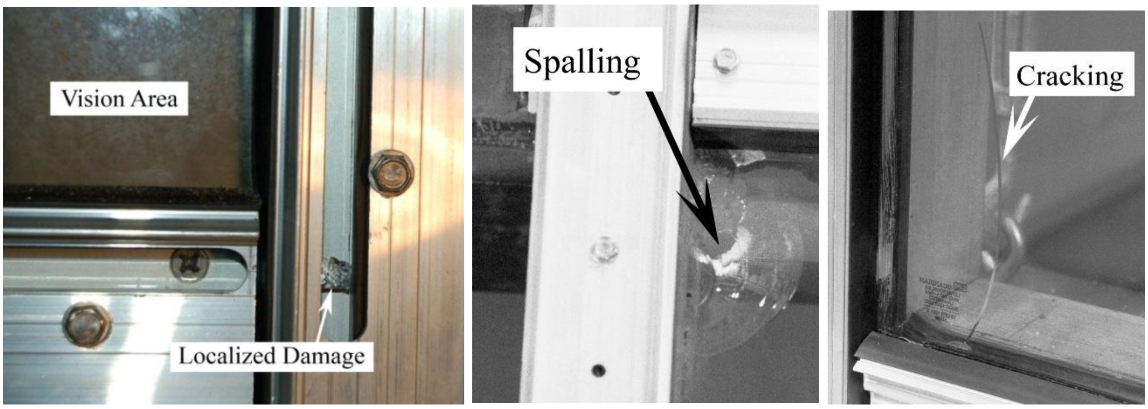

(a) (b) (c)

Fig. 2 Glass damage resulting from increasing lateral loading with depiction (a) showing crushing/spalling in non-vision area; (b) spalling in vision area; and (c) though-thickness crack in the vision area of the glass panel

2.2 Glass damage sates

While architectural glass systems can experience many different types of failure modes in a seismic event, this study focuses on the glass cracking damage state. The glass cracking failure is defined in this paper as the onset of glass crushing and cracking, which is characterized by initial corner crushing or through-thickness glass panel cracking in the vision or non-vision area of the panel. The vision area of a glass panel is considered the portion that is not covered by perimeter gaskets and pressure plates. Glass corner crushing and spalling in the non-vision portion of the glass panel can be seen in Fig. 2(a). Glass spalling and a through-thickness crack in the vision area of the glass panel can be seen in Figs. 2(b) and 2(c), respectively. The present definition of glass cracking damage in this paper differs from the definition in past studies (such as Behr *et al*. 1995, Behr 1998, and Memari *et al*. 2003), where the cracking damage state was defined as the drift amplitude causing a through-thickness crack in the glass panel vision region of the specimen.

In this paper, demands in the form of drift ratio as opposed to drift are utilized. The notation θ is used to signify drift ratio and δ is used to indicate drift, where drift ratio is defined as follows:

$$\theta = \frac{\delta}{h} \tag{5}$$

where h denotes the height over which the drift occurs.

3. Selected glass configurations

The research presented in this paper was aimed at developing a closed-form equation based on the laboratory data from a diverse set of glass curtain wall and storefront configurations that are commonly used on buildings and facilities today. Most of the data were obtained from experiments carried out by researchers over the past decade (Behr *et al*. 1995, Behr 1998, and Memari *et al*. 2003). Table 1 lists different curtain wall and storefront configurations that were selected for analysis, and for referencing throughout the report an identification number has been assigned to each assembly. A more detailed discussion on these configurations can be found in O'Brien *et al*. (2012), where new test data for Configurations 10 through 15 carried out as part of the research are also presented.

All configurations tested were dry-glazed, where rubber gaskets glaze the glass within the aluminum framing. Curtain wall glass panels were installed in a Kawneer 1600™ aluminum mid-rise framing system, and the storefront glass panels were installed in a Kawneer TriFab II® 450 or 451 aluminum framing system. The nominal glass-to-frame clearance for the curtain wall

Table 1 Summary of curtain wall and storefront glass configurations

ID	System	Glazing Type	Glass-To-Frame Clearance	Aspect Ratio	# of Spec.
1†	MR[1]	6 mm AN[3] monolithic	11 mm	6:5	7
2†	MR	25 mm AN IGU[4]	11 mm	6:5	7
3‡	MR	6 mm inner AN / 6 mm outer AN LAM[5] (0.030 PVB[6]) IGU	11 mm	6:5	6
4‡	MR	6 mm inner AN / 6 mm outer AN LAM (0.060 PVB) IGU	11 mm	6:5	6
5‡	MR	6 mm inner AN / 13 mm outer AN LAM (0.030 PVB) IGU	11 mm	6:5	6
6†	MR	6 mm AN LAM (0.030 PVB)	11 mm	6:5	24
7*	SF[2]	6 mm AN monolithic	10 mm	6:5	12
8*	SF	25 mm AN IGU	15 mm	6:5	12
9*	SF	6 mm AN LAM (0.030 PVB)	10 mm	6:5	12
10**	MR	6 mm AN monolithic	0 mm	6:5	2
11**	MR	6 mm AN monolithic	3 mm	6:5	2
12**	MR	6 mm AN monolithic	6 mm	6:5	3
13**	MR	25 mm AN IGU	6 mm	6:5	1
14***	MR	6 mm AN monolithic	11 mm	2:1	2
15***	MR	6 mm AN monolithic	11 mm	1:2	2
16†	MR	6 mm HS[7] monolithic	11 mm	6:5	8
17†	MR	25 mm HS IGU	11 mm	6:5	6
18†	MR	10 mm HS LAM (0.030 PVB)	11 mm	6:5	6
19‡	MR	6 mm inner AN / 6 mm outer HS LAM (0.060 PVB) IGU	11 mm	6:5	6
20‡	MR	6 mm inner AN / 13 mm outer HS LAM (0.060 PVB) IGU	11 mm	6:5	5
21†	MR	6 mm FT[8] monolithic	11 mm	6:5	6
22‡	MR	6 mm inner AN / 13 mm outer FT LAM (0.060 PVB) IGU	11 mm	6:5	6

[1]MR = mid-rise CW system with Kawneer 1600TM framing, [2]SF = storefront system with Kawneer TriFab II® 450 or 451 framing, [3]AN = annealed, [4]IGU = insulating glass unit, [5]LAM = laminated glass unit, [6]PVB = polyvinyl butyral, [7]HS = heat-strengthened, [8]FT = fully tempered

*Behr *et al*. 1996, †Behr 1998, ‡Memari *et al*. 2003, **O'Brien *et al*. 2012, ***not published specimens (except Configurations 10-13 in Table 1) was 11 mm, which is the recommended clearance for practical building installations. Recent experimental tests were conducted on curtain wall specimens with various substandard glass-to-frame clearances (glass Configurations 10-13 in Table 1) to help understand the seismic behavior of architectural glass with different clearances (O'Brien *et al*. 2012). For storefront configurations, the nominal glass-to-frame clearance for the 6 mm glass thickness types was 10 mm, while for the 25 mm glass thickness types the nominal clearance was 15 mm.

In-plane cyclic racking tests were performed on all glass configurations in Table 1. All curtain wall specimens were tested one at a time on the facility, while storefront configurations were tested three panels at a time (i.e., a 3-panel specimen). All specimens were tested according to the displacement-controlled racking protocol recommended in AAMA 501.6 (AAMA 2009) in a modified "stepwise" fashion. This test method is characterized by monotonically increasing-amplitude sinusoidal drift cycles that determine the serviceability drift limits and ultimate drift limits for architectural glass components subjected to cyclic, in-plane racking displacements. The test facility, setup, and testing protocol is described in greater detail in Behr and Belarbi (1996), Behr (1998), and Memari *et al*. (2003).

The selected glass systems include panels that are monolithic (Mono; panel composed of a single ply), laminated (Lami; panel composed of two glass plies with a polyvinyl butyral interlayer), and insulated glass unit (IGU; two panes with an air space in between). These glass panels may consist of annealed (AN), heat-strengthened (HT), or fully-tempered (FT) glass types. For the purposes of this research, configurations with IGU's are considered either symmetric (Sym; two glass panes are similar) or asymmetric (Asym.; two glass panes are different).

4. Development of a closed-form equation

4.1 Base equation development

To develop a new closed-form equation to predict the cracking capacity of a glass system, it is desirable to initially evaluate the accuracy of the ASCE equation by comparing the predicted glass cracking capacity calculated from the equation with actual drift values observed to cause cracking failure in the laboratory for the various glass configurations in Table 1. In the evaluation process, the accuracy was measured in terms of percent difference between predicted and experimental results as follows:

$$\%\,Diff. = \frac{\theta_{predicted} - \theta_{experimental}}{\theta_{experimental}}\,x100 \tag{6}$$

where $\theta_{predicted}$ denotes the drift ratio as found through Eq. (5) and $\theta_{experimental}$ denotes the experimental failure drift ratio value. The percent difference can be thought of as the inaccuracy of the predicted cracking failure relative to the experimental value.

For each glass configuration in Table 1, the cracking failure data for each specimen tested was input into Eq. (6) and a percent difference value determined. Then, an average of the percent differences was taken for the entire set of specimens for a given glass configuration. Finally, an overall average of the percent differences for all glass configurations was calculated using absolute value percentage values. The results of this analysis for each glass configuration type are presented in Table 2.

The results show that the average of the absolute percent differences for the 22 different glass configurations is 26.3%. Based on such a percent difference, it can be stated that the ASCE equation can predict glass cracking within approximately 26% error for the 22 glass configurations considered. The ASCE equation inaccuracy is bounded by underestimating the cracking failure of glass Configuration 10 by 100.0%, and overestimating the cracking capacity of glass Configuration 1 by 93.7%.

The amount of overall error can be considered relatively modest considering the random nature of glass cracking and variety of glazing frame properties that is not accounted for by the equation.

Table 2 Percent error comparison for ASCE 7 equation with experimental results

ID	$\theta^{crack}_{experimental}$	ASCE	
		$\theta^{crack}_{predicted}$	% Diff.
1	0.0138	0.0267	93.7%
2	0.0237	0.0267	13.0%
3	0.0279	0.0267	-4.2%
4	0.0270	0.0267	-1.0%
5	0.0270	0.0267	-1.0%
6	0.0161	0.0267	66.5%
7	0.0417	0.0253	-39.2%
8	0.0592	0.0372	-37.2%
9	0.0573	0.0253	-55.8%
10	0.0088	0.0000	-100.0%
11	0.0085	0.0076	-9.7%
12	0.0147	0.0153	3.9%
13	0.0142	0.0153	7.7%
14	0.0181	0.0273	51.1%
15	0.0220	0.0273	24.1%
16	0.0241	0.0267	10.8%
17	0.0266	0.0267	0.6%
18	0.0221	0.0267	20.7%
19	0.0261	0.0267	2.3%
20	0.0285	0.0267	-6.2%
21	0.0244	0.0267	9.8%
22	0.0332	0.0267	-19.5%
Average of Absolute Values[1]			26.3%

[1]This value represents the average of the absolute percentage difference values

As a result, the geometric relationship which models glass cracking that represents the glass-to-frame clearance and glass panel dimension characteristics within the ASCE equation is found to be reasonable. This finding guided the development of the new closed-form equation in this work to be formulated using ASCE 7-05 equation as a baseline equation to be modified considering additional glazing characteristics.

For the development of this equation, it is convenient to first present the ASCE equation (Eq. 3) consisting of two separate terms as shown in Eq. (7):

$$\Delta = 2c_1 + 2c_2\left(\frac{h}{b}\right) \tag{7}$$

where the variables are as previously defined.

4.2 Modification approach and factor development

An approach is taken where the set of available experimental failure values are analyzed to find trends in the data associated with various glazing and configuration characteristics that are known to affect glass capacity. Through comparison of failure data and in some cases the use of linear regression, the effect that a certain characteristic has on the failure values is identified, and trends or patterns are extracted from the data. Then, these trends are modeled and applied to the selected ASCE (baseline) equation in the form of a factor to account for the various forms of a particular glazing characteristic.

Initially, separate factors were developed for the glazing characteristics of glass material type (Φ_{type}) and glass configuration type (Φ_{config}) by modeling the effect that the particular characteristic has on glass cracking failure capacity relative to the capacity predicted by the baseline equation(which models glass-to-frame clearance and glass panel dimensions). The factors Φ_{type} and Φ_{config} were then directly applied to the baseline equation. The next three factors were developed separately based on trends observed affecting the capacity for that particular

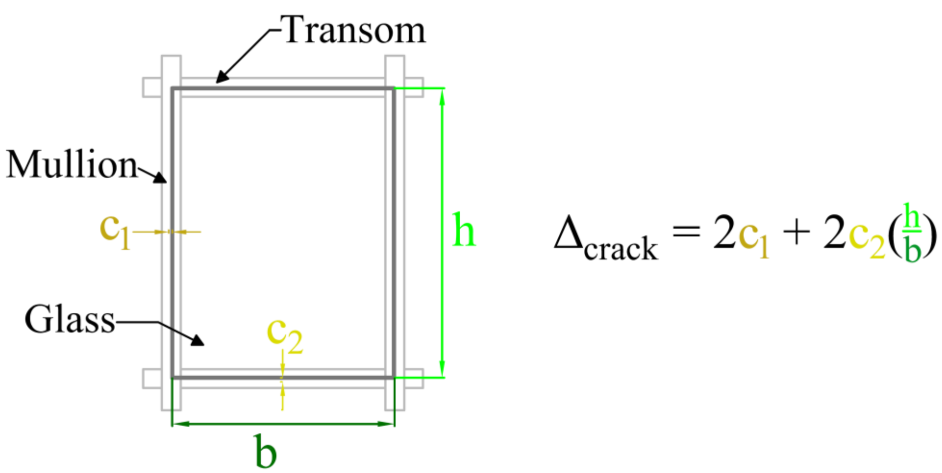

Fig. 3 Physical characteristics of glass-to-frame clearance and aspect ratio considered in the baseline equation

characteristic, but applied in terms of a partially revised equation (baseline equation with Φ_{type} and Φ_{config} factors applied). These factors include a factor to refine the baseline equation for modeling inaccuracies for substandard glass-to-frame clearances ($\Phi_{clearance}$) for clearances less than 11mm, a factor considering the type of system surrounding a glass panel (Φ_{system}), and a factor to refine the equation for modeling inaccuracies for varying glass panel aspect ratios. Fig. 3 illustrates the glazing characteristics considered in the baseline equation, to which the factors are subsequently applied.

4.2.1 Factor development: Φ_{type}

A glass type factor (Φ_{type}) is introduced in the closed-form equation since the experimental data indicates that the capacity of a curtain wall glass configuration generally increases as the glass material strength increases from annealed (AN) to heat-strengthened (HS) to fully-tempered (FT). This trend is shown in Figure 4, where the experimental glass cracking failure drift ratios for the four glass configuration types of monolithic (mono), laminated (lami), unsymmetric insulating glass unit (unsym. IGU) and symmetric insulating glass unit (sym. IGU) are plotted against glass types AN, HS, and FT. The experimental capacity presented for any glass configuration listed in Table 1 was determined by averaging the experimental failure values of all the test specimens for that particular configuration. To isolate the glass type effects on the failure values, only the data from curtain wall glass Configurations 1-6, 16-21, and 24 in Table 1 with standard glass-to-frame clearances of 11 mm and glass panel dimensions of 1.5 m wide by 1.8 m high were considered.

In Fig. 4, a line connecting the data points for a particular configuration highlights the effect of a particular glass type on the capacity. The predicted cracking drift ratio as calculated using the ASCE equation is shown by the dotted line, whose value remains constant.

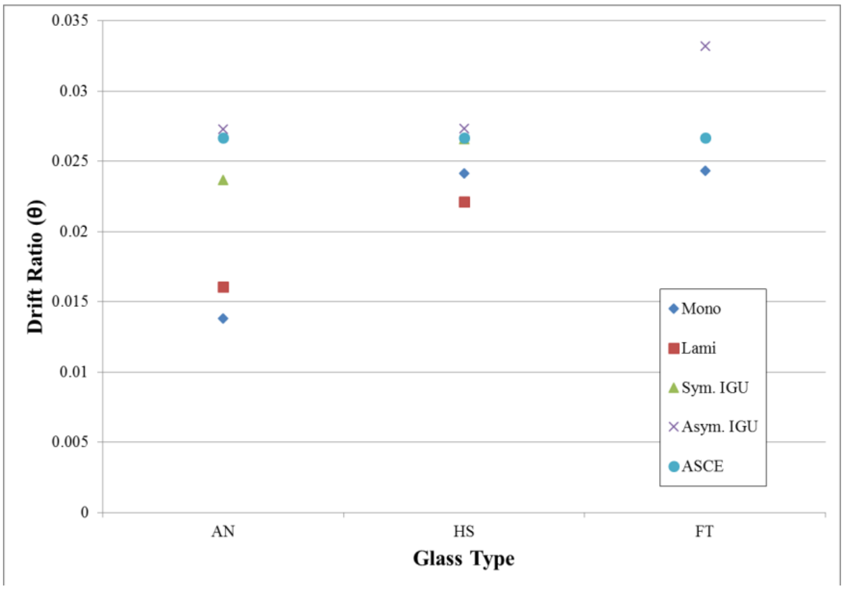

Fig. 4 Experimental glass cracking failure drift ratios for different glass panel configuration types plotted against glass type and compared with predicted cracking drift ratio failure from the ASCE equation

Values of Φ_{type} factor are developed for a discrete set of variables, AN, HS, and FT glass types. The magnitude of the factor for each glass type is determined by averaging the effect of a particular glass type across all configurations. The quantified effect is then divided by the predicted capacity from the baseline equation as follows:

$$\Phi^{x}_{type} = \frac{\theta^{x_{ave}}_{exp}}{\theta_{base}} \tag{8}$$

where Φ^{x}_{type} denotes the factor value for a given glass type x [x = AN, HS, or FT], $\theta^{x_{ave}}_{exp}$ the average experimental drift ratio of the four configurations with glass type x as defined by Eq. (9), and θ_{base} the cracking drift ratio as presumed to be predicted by the baseline ASCE equation.

$$\theta^{x_{avg}}_{exp} = \frac{\theta^{x_{mono}}_{exp} + \theta^{x_{lami}}_{exp} + \theta^{x_{sym-IGU}}_{exp} + \theta^{x_{asym-IGU}}_{exp}}{4} \tag{9}$$

The calculated factor values using Eqs. (8) and (9) are presented in Table 3. The observed trend in the experimental data where experimental capacity increased from AN to HS to FT glass types is reflected in these factor values. The application of Φ_{type} to the baseline equation is presented in Eq. (10).

$$\Delta_{crack} = \Phi_{type}\left[2c_1 + \left(2c_2\left(\frac{h}{b}\right)\right)\right] \tag{10}$$

It should be noted that experimental data for laminated and symmetric IGU configuration types with FT glass were not available at the time of the study. To keep a statistical balance when performing factor value calculations for the FT glass type, it was assumed that the experimental glass cracking capacity for FT-Lami and FT-IGU configuration systems were equivalent to the capacity determined experimentally for these configuration with HS glass. This is a conservative assumption (as FT glass has higher strength than HS glass) until a more accurate development of the FT glass type factor value is developed. Follow-up testing on these configurations with FT glass could produce experimental values which can be used to refine the FT Φ_{type} value.

4.2.2 Factor development: Φ_{config}

Trends are additionally observed in the data illustrated in Figure 4 that cracking failure capacity is affected by glass configuration justifying the development of a factor (Φ_{config}) to account for this glazing characteristic. IGU configurations (symm. or asym.) generally have greater experimental cracking failure values than laminated or monolithic configuration types. To isolate the effect of configuration, only the data from curtain wall glass Configurations 1-6, 16-21, and 24 in Table 1 with standard glass-to-frame clearances of 11 mm and glass panel dimensions of 1.5 m wide by 1.8 m high are considered.

Values for the Φ_{config} factor are developed for the discrete set of configurations Mono, Lami, sym. IGU, and asym. IGU. The effect of a glass configuration type is quantified by averaging the effect of a particular glass configuration type across all three glass types (AN, HS, and FT). Then, this quantified effect is divided by the predicted drift ratio from the baseline equation, as follows:

$$\Phi^{x}_{config} = \frac{\theta^{x_{ave}}_{exp}}{\theta_{base}} \tag{11}$$

Table 3 Developed Φ_{type} factor values for glass cracking limit state predictions

	$\mathbf{\Phi}_{type}$
AN	0.76
HS	0.94
FT	0.99

Table 4 Developed Φ_{config} factor values for glass cracking limit state predictions

	$\mathbf{\Phi}_{config}$
Mono	0.78
Lami	0.75
Sym. IGU	0.96
Asym. IGU	1.10

where Φ^{x}_{config} denotes the factor value for a given configuration type x [x = Mono, Lami, sym. IGU, or asym. IGU], $\theta^{x_{ave}}_{exp}$ is the average experimental drift ratio of the three glass types with configuration type x as defined by Eq. (12), and θ_{base} is the cracking drift ratio as predicted by the baseline ASCE equation.

$$\theta^{x_{avg}}_{exp} = \frac{\theta^{x_{AN}}_{exp} + \theta^{x_{HS}}_{exp} + \theta^{x_{FT}}_{exp}}{3} \tag{12}$$

The calculated Φ_{config} factor values using Eqs. (11) and (12) are presented in Table 4. These factor values support the trend indicated previously in the experimental data where the experimental capacity for both IGU configuration types is greater than the values for monolithic and laminated types. Since the experimental data for laminated and symmetric IGU's configuration types with FT glass were not available as noted before, when calculating the factor value for the Lami and sym. IGU configuration types, it was conservatively assumed that the FT-Lami and FT-IGU systems had an experimental capacity equal to similar configurations with HS glass (as mentioned previously FT glass has higher strength than HS glass). The application of Φ_{config} to the baseline equation is presented in Eq. (13).

$$\Delta_{crack} = \Phi_{config}\left[2c_1 + \left(2c_2\left(\frac{h}{b}\right)\right)\right] \tag{13}$$

Up to this point, the developed equation with the application of both Φ_{type} and Φ_{config} factors is represented by Eq. (14). The factors effect on accuracy of the equation is summarized following the factor development sections.

4.2.3 Factor development: $\Phi_{clearance}$

The analysis of experimental data indicated that the drift capacity at some glass-to-frame clearances below the standard 11 mm was greater than that predicted with the ASCE equation. In Fig. 5 the cracking failure data for AN monolithic configurations with standard and substandard clearances are plotted. The figure indicates that the experimental capacity gradually decreases as the clearance decreases. If the predicted capacity from the ASCE equation is plotted for comparison, a trend emerges where the ASCE equation goes from significantly overestimating the capacities for the configuration with the standard clearance to significantly underestimating the configurations with the lowest clearances. This greater than expected failure capacity of configurations with substandard clearances has been observed in earlier published research (O'Brien *et al*. 2012), where it was concluded that the absence of the larger gap inhibits glass edge contacts with the metal framing, thereby permitting the glass panels to crack at greater than expected drift values. As a result, a factor is developed to refine the baseline model to account for the different failure behavior of glass configurations with sub-standard clearances. While a sub-standard clearance in a system may not be recommended for other reasons, it is desirable to be able to accurately model the seismic response of systems with sub-standard clearances since it is possible that these may exist even if not by design.

This general trend does not change when the experimental results are compared with the predicted drift ratios obtained from the revised baseline equation with application of the developed factors (see Eq. (14)). This trend is seen in Fig. 6, which contains plots from the drift ratio values as predicted from the modified baseline equation (Eq. 14) and experimental values according to the glass-to-frame clearance.

Since the baseline equation already contains glass-to-frame clearances (c_1 and c_2), the clearance factor ($\Phi_{\text{clearance}}$) was formulated to correct the underestimation in capacity based on the observed trends. Additionally, since there is no discrete set of substandard glass-to-frame clearance values, the $\Phi_{\text{clearance}}$ factor is best formulated as a function of a clearance range. The $\Phi_{\text{clearance}}$ factor is developed such that this trend is reflected by refining the model in relation to the revised baseline equation with application of both Φ_{type} and Φ_{config} factors (Eq. 14), as follows:

$$\Delta_{crack} = \Phi_{type}\Phi_{config}\Phi_{clearance}\left[2c_1 + \left(2c_2\left(\frac{h}{b}\right)\right)\right] \tag{15}$$

To accomplish this, first an initial set of clearance-specific $\Phi_{\text{clearance}}$ factor values were determined, where a clearance-specific $\Phi_{\text{clearance}}$ factor value is determined for a given glass configuration with specific glass-to-frame clearance. These values were calculated using Eq. (16), where the underestimated portion of a glass configuration's experimental capacity with a given substandard glass-to-frame clearance was added to the predicted drift, the sum was equated to Eq. (15), and $\Phi_{\text{clearance}}$ values were solved for. It should be noted that the variables were normalized into drift ratios for the calculations, but are denoted as drifts for illustrative purposes.

$$\begin{aligned} &\Delta_{crack} + \Delta_{sub-clearance} = \Phi_{type}\Phi_{config}\Phi_{clearance}\left[2c_1 + \left(2c_2\left(\frac{h}{b}\right)\right)\right] \\ &\rightarrow \Phi_{clearance} = \frac{\Delta_{crack} + \Delta_{sub-clearance}}{\Phi_{type}\Phi_{config}\left[2c_1 + \left(2c_2\left(\frac{h}{b}\right)\right)\right]} \end{aligned} \tag{16}$$

where Δ_{crack} denotes the predicted capacity from Eq. (14), and $\Delta_{\text{sub-clearance}}$ denotes the amount by which the experimental failure drift capacity is underestimated by Eq. (14) and is determined as follows:

$$\Delta_{sub-clearance} = \left(\Delta_{standard}^{pred} - \Delta_{x}^{pred}\right) - \left(\Delta_{standard}^{exp} - \Delta_{x}^{exp}\right) \tag{17}$$

where $\Delta_{standard}^{pred}$ denotes the predicted cracking drift for a glass configuration with a standard 11 mm clearance by Eq. (14), Δ_{x}^{pred} denotes the predicted drift (using Eq. 14) for a similar system with a given substandard clearance x, $\Delta_{standard}^{exp}$ denotes the experimentally observed cracking drift value for a glass configuration with a standard 11 mm clearance, and Δ_{x}^{exp} denotes the experimentally observed drift value for a similar system with a substandard clearance x.

Using Eq. (16), the clearance-specific $\Phi_{clearance}$ factor values were found for glass Configurations 1, 11, and 12 as shown in Table 5.

The data from glass Configuration 10 with a glass-to-frame clearance of 0 mm is not included since the failure behavior was experimentally more erratic compared to glass configurations with clearances greater than zero, and as a result is considered a statistical anomaly. Additionally, the data from AN-Mono glass Configuration 1 with a standard 11 mm glass-to-frame clearance was included because it provides a relation of the data points with the other substandard clearances to the results of a configuration with a 11 mm standard clearance.

Table 5 Calculated preliminary factor values from Equation (16) for glass Configurations 1, 11, and 12

Config. ID	Clearance (mm)	Clearance-Specific $\Phi_{clearance}$
1	11	1.02
12	6	1.81
11	3	2.34

Fig. 5 Glass cracking failure drift ratio versus glass-to-frame clearance for AN-Mono glass configuration – experimental values compared to predicted values

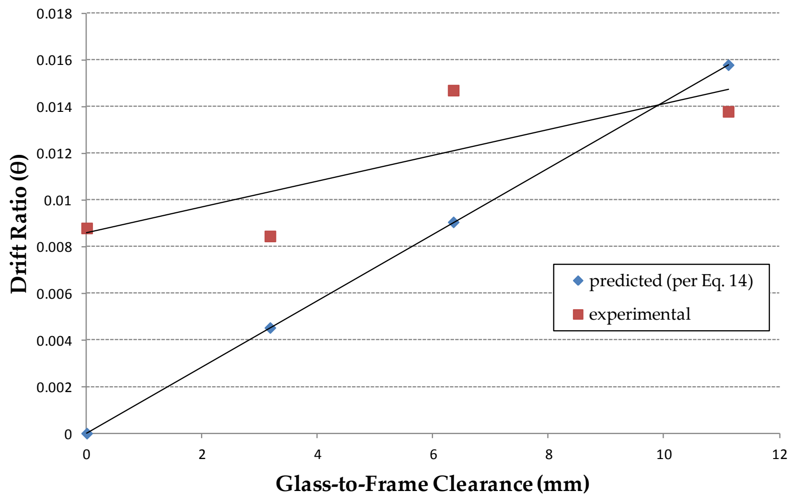

Fig. 6 Plotted modified baseline equation (Eq. 14) predicted and experimental drift ratios with corresponding best-of-fit lines

With clearance-specific $\Phi_{clearance}$ factor values determined, the next step was to evaluate whether a statistical relationship exists between these factor values and the glass-to-frame clearance values of a given glass configuration. A regression analysis demonstrated that an almost linear relationship was found to exist between the glass-to-frame clearance values and the calculated clearance-specific factor values for glass Configurations 1, 11, and 12 as seen in Fig. 7. This conclusion is reflected by the coefficient of determination value (R^2) equivalent to 0.998. A perfect linear relationship exists between two variables when an R^2 value equals 1.0. The authors recognize that the linear regression analysis is based on a limited number of data points, but as more test data become available, the factors can be further refined.

Since the glass-to-frame clearance value was very highly correlated with the clearance-specific $\Phi_{clearance}$ values, and it is desired to formulate a $\Phi_{clearance}$ factor as a function of a given clearance value, the linear equation y = -0.1673x + 2.8741 is desirable to be approximated to determine the $\Phi_{clearance}$ factor as follows:

$$\Phi_{clearance} = -0.17x + 2.87 \geq 1.0 \tag{18}$$

where x is equivalent to the glass-to-frame clearance (in mm) of a given configuration. The limit placed on $\Phi_{clearance}$ implies that the factor is intended only to apply for glass configurations with substandard clearances (less than 11mm).

It is proposed that for glass configurations with a glass-to-frame clearance below 3 mm, the capacity of the glass configuration be calculated using a 3 mm clearance dimension value for the closed-form equation and $\Phi_{clearance}$ factor. As defined, the ASCE and Eq. (14) predicts a glass capacity of 0.00 (drift ratio) for configurations with a glass-to-frame clearance of 0 mm. However, the experimental cracking drift ratio failure for Configuration 10 with a glass-to-frame clearance of zero is 0.0088 (see Table 2). This is nearly equivalent to the capacity of 0.0085 for the similar Configuration 11 with a 6 mm clearance. It is conceivable that configurations other than AN-

Mono with clearances between 0 mm and 6 mm could follow a similar trend, but further experimental work will be needed to evaluate this possibility.

4.2.4 Factor development: Φ_{system}

Due to the different framing and glazing detailing of storefront systems as well as their anchorage to structural members where they are placed within the wall or frame opening, storefront systems exhibit different response compared with mid-rise curtain wall systems that are normally hung and offset from the plane of the structural frame. Overall, the experimental data indicate that unlike older storefront systems that have been vulnerable to earthquake damage, modern storefront systems have significantly greater drift capacity compared to curtain wall systems with similar configurations. This trend is shown in Fig. 8, where the predicted capacity from the ASCE equation is also shown for reference.

In addition to the trend comparing storefront to curtain wall values, it can be inferred from the analysis that the glass cracking drift ratios for storefront systems are significantly greater than the predicted ASCE values. To formulate the Φ_{system} factor to account for this trend and determine the magnitude of the values, a comparison analysis was conducted that relates the predicted and experimental drift ratios for storefront Configurations 7-9. Table 7 summarizes the analysis, where Column A lists the predicted cracking drift ratio from modified baseline Eq. (14) without Φ_{system} factor, Column B the experimental drift ratio, and Column C the ratio of Column B to A.

Table 6 Example $\Phi_{clearance}$ factor values based on application of Eq. (18)

Clearance (mm)	$\Phi_{clearance}$
13	1.0
11	1.0
6	1.85
3	2.36
0	2.36

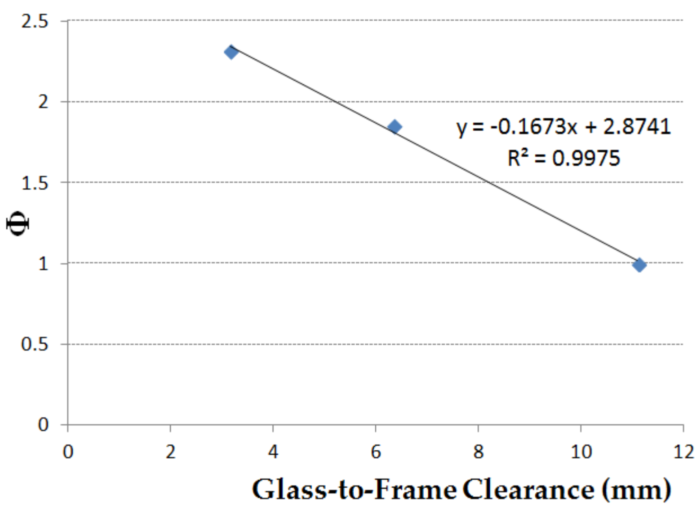

Fig. 7 Relationship between clearance-specific $\Phi_{clearance}$ values and glass-to-frame clearance values

Table 7 shows that the ratios in Column C vary across the storefront Configurations (7-9) and are between 2.18 and 3.98, which means that the experimental results are double to quadruple the cracking drift ratios estimated by the closed-form equation. Overall, the revised closed-form equation underestimates the cracking drift capacity of storefront glass Configurations 7-9 by an average of 64.0%. The magnitude of Φ_{system} for storefront systems should preferably utilize the lowest factor value (from Table 7), such that a general Φ_{system} factor value for storefront systems does not overestimate the capacity. It is suggested a Φ_{system} factor value of 2.15 be used for storefront systems, as shown in Table 8. The authors recognize that further experimental data will be needed to refine the factor values further.

The Φ_{system} factor will then be applied to the revised closed-form equation as follows:

$$\Delta_{crack} = \Phi_{type}\Phi_{config}\Phi_{system}\left[2c_1 + \left(2c_2\left(\frac{h}{b}\right)\right)\right] \tag{19}$$

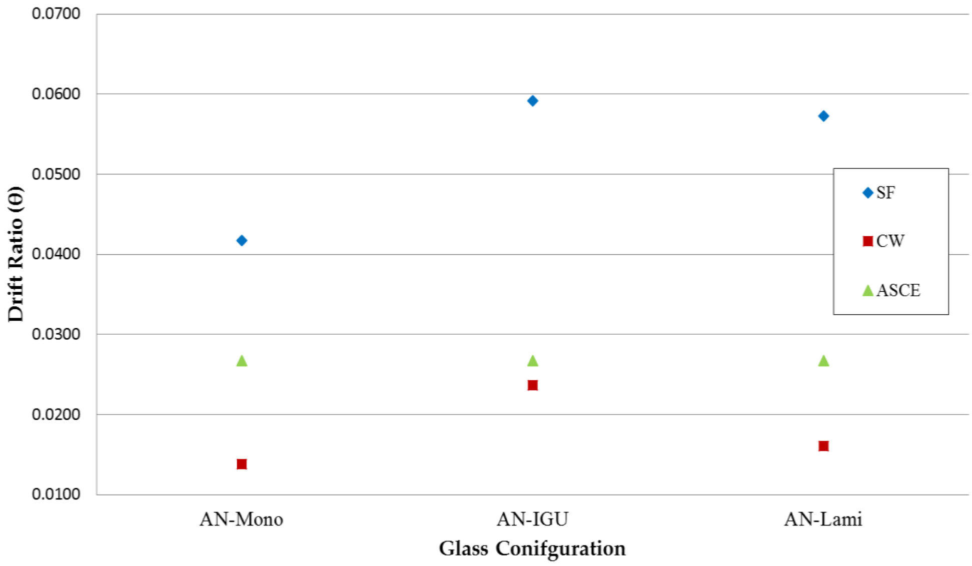

Fig. 8 Glass cracking failure drift ratio versus glass configuration for AN-Mono, AN-IGU, and AN-Lami glass configurations – SF experimental values compared with data for comparable CW configurations and the predicted values from ASCE equation (Eq. 3)

Table 7 Comparison of predicted and experimental glass cracking drift ratios for storefront configurations

	A	B	C
Config. ID	$\theta_{predicted}$	$\theta_{experimental}$	$\dfrac{\theta_{experimental}}{\theta_{predicted}}$
7	0.0150	0.0417	2.78
8	0.0271	0.0592	2.18
9	0.0144	0.0573	3.98

Table 8 Values of the Φ_{system} factor

System Type	Φ_{system}
CW	1.0
SF	2.15

4.2.5 Factor development: Φ_{aspect}

A factor Φ_{aspect} is developed to refine modeling inaccuracies present in the baseline equation as the aspect ratio (height/width or *h*/*b*) of a glass panel changes, represented in the baseline equation by the variables *h* (height) and *b* (width) of a glass panel. Most of the glass configurations tested experimentally had a glass aspect ratio of 6:5, with a glass panel height of 1.8 m and width of 1.5 m. However, glass Configurations 14 and 15 have aspect ratios of 2:1 and 1:2, respectively, and an analysis of the experimental results of these two configurations was performed. The glass cracking failure data from two tests on AN-Mono glass configurations with 2:1 (2.4 m high by 1.2 m wide) and 1:2 (1.2 m high by 2.4 m wide) glass panel aspect ratios were compared with an AN-Mono (Configuration 1) that is similar, but with a 6:5 aspect ratio, to isolate the physical characteristic of aspect ratio. The experimental data show that compared to the result for the 6:5 aspect ratio, the drift capacity for 2:1 and 1:2 aspect ratios increase as the glass aspect ratio increases or decreases from 6:5. This condition is shown in Fig. 9, where the ASCE predicted values are also plotted and as shown do not adequately model the aspect ratio. While the values forASCE are lowest for 6:5 aspect ratio as observed with the experimental results, overall the ASCE values are significantly greater than the experimental results and do not reflect the significantly greater changes in capacity as seen in the experimental results as a result of a varying aspect ratio.

Glass dimensions affect the capacity of glass systems intrinsically since drift measurements are defined as the horizontal displacement over a considered height. Therefore, as the height of a considered glass panel increases as the width remains the same, the drift capacity as predicted by the baseline ASCE equation increases. This effect is normalized as drifts are converted to drift ratios (defined as drift over height that a drift occurs). Given the dimensions of glass configurations 1, 14, and 15, the predicted capacity in terms of drift ratio by the baseline equation is approximately the same for all three configurations. However, Configurations 14 and 15 had greater experimental capacity compared to Configuration 1, suggesting that the seismic response behavior of glass configurations with aspect ratios greater or less than 1.0 are slightly different than glass configurations with an aspect ratio near 1.0. Glass panels with aspect ratios significantly greater or less than 1.0 may rotate to less relative to glass panels with aspect ratio of 1.0 when subjected to lateral displacements, delaying glass panel contact with the framing and therefore increasing the cracking resistance of these configurations.

An analysis was then performed to compare the predicted capacity between the revised closed-form equation that additionally accounts for glass type and glass configuration (Eq. 14) and the experimental results for Glass Configurations 14 and 15 (including Glass Configuration 1). The results are summarized in Fig. 10, which shows that the predicted cracking capacity (based on Eq. 14) is not sensitive to aspect ratio (as would be expected based on the data comparison in Fig. 9 with the ASCE Eq. 3). Additionally, the predicted capacity underestimates the experimental failure results for Configurations 14 and 15.

In Fig. 10, data relationships are characterized by two different slopes of lines connected by points in the experimental data series; each one originates at glass Configuration 1 with a 6:5

aspect ratio and extends upward to the experimental drift ratio for glass Configurations 14 and 15 with a 2:1 and 1:2 aspect ratio, respectively. Since the slopes of these two linear relationships are not similar, the Φ_{aspect} factor will be formulated considering two separate relationships. One definition will address situations where aspect ratios are greater than 6:5, and the other less than 6:5.

Since glass panel dimensions h and b are only represented in the second term of the equation, the Φ_{aspect} factor is formulated so that it is only applied to the second term of the base equation. The Φ_{aspect} factor will be applied to revise the closed-form equation as follows:

$$\Delta_{crack} = \Phi_{type}\Phi_{config}\left[2c_1 + \Phi_{aspect}\left(2c_2\left(\frac{h}{b}\right)\right)\right] \tag{20}$$

The Φ_{aspect} factors are initially determined by adding the experimental failure capacity underestimated by Eq. (14) to the left side of Eq. (20), and solving for Φ_{aspect} as follows:

$$\begin{aligned} &\Delta_{crack} + \Delta_{aspect} = \Phi_{type}\Phi_{config}\left[2c_1 + \Phi_{aspect}\left(2c_2\left(\frac{h}{b}\right)\right)\right] \\ &\rightarrow \Phi_{aspect} = \frac{\Delta_{crack} + \Delta_{aspect} - \Phi_{type}\Phi_{config}2c_1}{\Phi_{type}\Phi_{config}2c_2\left(\frac{h}{b}\right)} \end{aligned} \tag{21}$$

Table 9 Calculated initial factor values

Config. ID	Aspect Ratio	Initial Φ_{aspect}
15	0.5	2.46
1	1.2	1.00
14	2.0	1.36

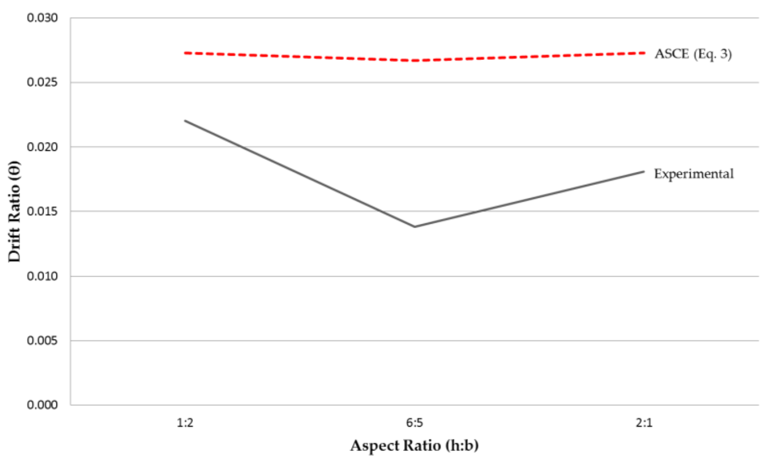

Fig. 9 Plotted experimental and predicted cracking drift ratios for AN-Mono configurations with 1:2, 6:5, and 2:1 aspect ratios

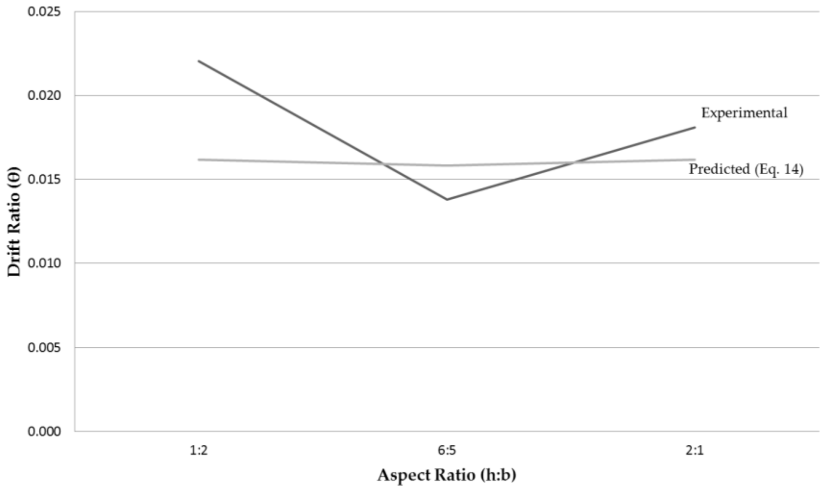

Fig. 10 Comparison between experimental failure values and predicted (Eq. 14) glass cracking values with corresponding aspect ratio for a given AN-Mono glass configuration

Table 10 Sample values for the Φ_{aspect} factor for various aspect ratios

Aspect Ratio	Φ_{aspect}
1:2 (0.5)	2.46
3:4 (0.75)	1.93
6:5 (1.2)	1.0
3:2 (1.5)	1.14
2:1 (2.0)	1.36

where Δ_{crack} denotes the predicted capacity from Eq. (14) for a given glass configuration, and Δ_{aspect} as determined from Eq. (22) denotes the experimental drift increase as caused by a given glass panel aspect ratio relative to a similar configuration with a reference 6:5 aspect ratio that is not accounted for by the equations.

$$\Delta_{aspect} = \left(\Delta_x^{exp} - \Delta_{6:5}^{exp}\right) - \left(\Delta_x^{pred} - \Delta_{6:5}^{pred}\right) \tag{22}$$

where Δ_x^{exp} denotes the experimental cracking drift for a glass configuration with a given aspect ratio *x*, $\Delta_{6:5}^{exp}$ denotes the experimental drift for a similar configuration with a reference 6:5 aspect ratio, Δ_x^{pred} denotes the predicted cracking drift for a glass configuration with a given aspect ratio x, and $\Delta_{6:5}^{pred}$ denotes the predicted drift for a similar configuration with a standard 6:5 aspect ratio.

Using Eq. (21), the initial Φ_{aspect} factor values for glass Configurations 1, 14, and 15 are calculated and presented in Table 9:

The second primary step in the factor formulation is to develop two separate linear relationships between the aspect ratio values and initial factor values found for Configurations 14 and 15 with respect to the glass Configuration 1 data, where a factor value of 1.0 is assumed for glass Configurations 1 with a reference aspect ratio of 6:5. The linear relationships produce equations that will relate any given aspect ratio value with an appropriate factor value. The first relationship shown in Fig. 11(a) was created for instances where the aspect ratio of a given glass configurations is less than 6:5 (1.2), and was based on the data point sets from Configurations 15

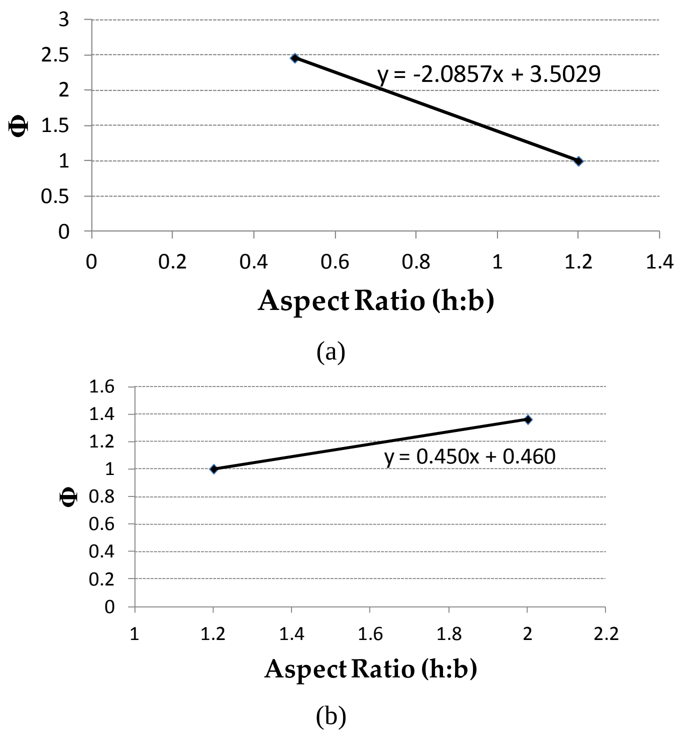

Fig. 11 Developed linear equations based on data in Table 9 for (a) configurations (1) and (15) that account for aspect ratios less than standard (6:5) and for (b) configurations (1) and (14) that account for aspect ratios greater than standard (6:5)

and 1. The other relationship in Fig. 11(b) was created for the instances where the aspect ratio of a given glass configuration is more than 6:5 (1.2), and was based on the data point sets from Configurations 14 and 1. As alluded to earlier, further research will be needed to contribute additional data for refinement of the factor values.

Finally, the last primary step is to define Φ_{aspect} factor values based on the linear equations just described. Using the linear relationships seen in Fig. 11(a) and 11(b), the values were rounded so that the Φ_{aspect} factor is defined by Eq. (23):

$$\Phi_{aspect} = \begin{cases} \text{if aspect ratio} \leq 6:5, \text{then}: \Phi = -2.09\left(\frac{h}{b}\right) + 3.5 \\ \text{if aspect ratio} > 6:5, \text{then}: \Phi = 0.45\left(\frac{h}{b}\right) + 0.46 \end{cases} \tag{23}$$

As an example of factor values that result from the Φ_{aspect} factor definition, a sample set of aspect ratios is input into Eq. 23 and the resulting values are organized in Table 10.

4.2.6 Factor development: $\Phi_{connection}$

To account for the effects that a varied framing-to-structure connection has on the cracking seismic capacity of glass configurations in the closed-form equation, another factor is needed. In

Table 11 Accuracy of closed-form equation with the application of Φ_{type} and Φ_{config} factors compared with accuracy of the base equation*

A	B	C	D	E	F		G	
System	Config.ID	θ_{base}	Φ_{type}	Φ_{config}	Cracking		% Difference	
					θ_{pred}	θ_{exp}	Eq. 14	ASCE
AN-Mono	1	0.0267	0.76	0.78	0.0159	0.0138	14.8%	93.7%
AN- IGU (sym.)	2	0.0267	0.76	0.96	0.0195	0.0237	-17.6%	13.0%
AN-IGU (asym.)	3-5	0.0267	0.76	1.10	0.0224	0.0273	-18.2%	-2.1%
AN-Lami	6	0.0267	0.76	0.75	0.0152	0.0161	-5.1%	66.5%
HS-Mono	16	0.0267	0.94	0.78	0.0196	0.0241	-18.8%	10.8%
HS-IGU (sym.)	17	0.0267	0.94	0.96	0.0241	0.0266	-9.2%	0.6%
HS-Lami	18	0.0267	0.94	0.75	0.0188	0.0221	-14.9%	20.7%
HS-IGU (asym.)	19, 20	0.0267	0.94	1.10	0.0276	0.0273	1.1%	-2.2%
FT-Mono	21	0.0267	0.99	0.78	0.0206	0.0244	-15.2%	9.8%
FT-IGU (asym.)	24	0.0267	0.99	1.10	0.0291	0.0332	-12.3%	-19.5%
Average of Absolute Values[1]							12.7%	23.9%

*Note: The results are normalized and given in drift ratios where the predicted drift from the term is divided by the height of the configuration's glass panel

[1]This value represents the average of the absolute percentage difference values

the test setup used for experimental studies mentioned previously, the frame-to-facility connection was rigid and had negligible rotation. However, connections in the field may have semi-rigid characteristics, where the flexibility may vary from one type of connection to the next. Until laboratory testing is performed on various common connection types, the values of $\Phi_{connection}$ cannot be determined. It is assumed that the factor will add capacity to glass configurations, since the less rigid a connection is, the more rotation is allowed and subsequently the glass configuration will be able to withstand larger displacements before failure.

Since the factor $\Phi_{connection}$ represents a glass system detail that affects the entire glass configuration, it will be applied to the entire equation. With the addition of the factor, the equation will have the following form:

$$\Delta_{crack} = \Phi_{type}\Phi_{config}\Phi_{clearance}\Phi_{system}\Phi_{connection}\left[2c_1 + \Phi_{aspect}\left(2c_2\left(\frac{h}{b}\right)\right)\right] \tag{24}$$

For now, the factor $\Phi_{connection}$ will have a neutral, assumed value of 1.0. This value can be onsidered conservative since it assumes any given configuration to have rigid connections.

4.2.7 Individual factor accuracy analysis

During the development of the proposed closed-form equation, accuracy analyses were performed following the application of the Φ_{type} and Φ_{config} factors to the baseline equation, and

Table 12 Accuracy of partially revised equation with the application of $\Phi_{clearance}$, Φ_{system} and Φ_{aspect} factors compared with accuracy of the partially revised Eq. 14*

A	B	C	D	E	F	G	H		I	
Config. ID	Eq. 14	Φ_{type}	Φ_{config}	$\Phi_{clearance}$	Φ_{system}	Φ_{aspect}	Cracking		% Difference	
							θ_{pred}	θ_{exp}	Eq. 15	Eq. 14
				$\Phi_{clearance}$						
10	0.0000	0.76	0.78	2.36	n/a	n/a	0.0107	0.0088	21.4%	100%
11	0.0076	0.76	0.78	2.36	n/a	n/a	0.0107	0.0085	25.7%	-46.7%
12	0.0152	0.76	0.78	1.85	n/a	n/a	0.0168	0.0147	14.0%	-38.3%
13	0.0152	0.76	0.96	1.85	n/a	n/a	0.0206	0.0142	45.2%	-21.8%
			Average of Absolute Values[1]						26.6%	51.7%
				Φ_{system}					Eq. 19	
7	0.0253	0.76	0.78	1.17	2.15	n/a	0.0378	0.0417	-9.4%	-64.0%
8	0.0372	0.76	0.96	1.0	2.15	n/a	0.0583	0.0592	-1.6%	-53.3%
9	0.0253	0.76	0.78	1.17	2.15	n/a	0.0363	0.0573	-36.6%	-74.8%
			Average of Absolute Values[1]						15.9%	64.0%
				Φ_{aspect}					Eq. 20	
14	0.0273	0.76	0.78	n/a	n/a	1.36	0.0201	0.0181	11.0%	-10.4%
15	0.0273	0.76	0.78	n/a	n/a	2.46	0.0241	0.0220	9.4%	-26.4%
			Average of Absolute Values[1]						10.2%	18.4%

*Note: The results are normalized and given in drift ratios where the predicted drift from the term is divided by the height of the configuration's glass panel

[1]This value represents the average of the absolute percentage difference values

again following application of each $\Phi_{clearance}$, Φ_{system} and Φ_{aspect} factor to the partially revised baseline equation (Eq. 14) to evaluate the sensitivity of the prediction to these factors. For the Φ_{type} and Φ_{config} factors, the accuracy is evaluated by finding the percent difference of the predicted drift ratios (Eq. 14) of a given glass system with respect to the experimental results.

The analysis and results are shown in Table 11 where Column A denotes a given glass system, Column B the glass configuration ID, Column C the predicted drift ratio from the baseline equation (Eq. 3), Columns D and E the applicable values for Φ_{type} and Φ_{config}, respectively, Column F the drift ratio using Eq. (14) in comparison with the experimental drift ratio, and Column G the percent difference between both the values from Eq. (14) and baseline equation (Eq. 3) with respect to the experimental results. For the glass systems where more than one glass configuration listed in Table 1 applies, the data were weighted equally among applicable glass configurations for all evaluations. Overall, the analysis shows that the application of the factors decreases the percent difference of the predicted values relative to the experimental values from 23.9% (based on Eq. (3)) to 12.7% (based on Eq. (14)) for the applicable configurations in the analysis.

For the $\Phi_{clearance}$, Φ_{system} and Φ_{aspect} factors, the accuracy is evaluated by finding the percent difference of the predicted drift ratios of a given glass system with respect to the experimental results. Initially, the predicted drift ratio is calculated from the revised baseline equation (Eq. 14). The analysis and results are shown in Table 12 where Column A denotes a given glass configuration, Column B the predicted drift ratio from the revised baseline equation (Eq. 14), Columns C-G the applicable values for factors, Column H the predicted drift ratio using Eq. (15), Eq. (19), or Eq. (20) (for the separate $\Phi_{clearance}$, Φ_{system} and Φ_{aspect} factor evaluations) in comparison with the experimental drift ratio, and Column G the percent difference between both the values from the applicable revised equation (15, 19, or 20) and partially revised baseline equation (Eq. 14) with respect to the experimental results. Overall, the analysis shows that the application of the factors decreases the percent difference of the predicted values relative to the experimental values from 51.7% (based on Eq. (14)) to 26.6% (based on Eq. (15)) for $\Phi_{clearance}$, from 64.0% (based on Eq. (14)) to 15.9% (based on Eq. (19)) for Φ_{system}, and from 18.4% (based on Eq. (14)) to 10.2% (based on Eq. (20)) for Φ_{aspect} for the applicable configurations in the analysis.

Table 13 Summary of factors employed in the closed-form equation to estimate the horizontal drift causing glass cracking

Factor	Definition
Closed-Form Equation	$\Delta_{crack} = \Phi_{type}\Phi_{config}\Phi_{clearance}\Phi_{system}\Phi_{connection}\left[2c_1 + \Phi_{aspect}\left(2c_2\left(\frac{h}{b}\right)\right)\right]$
Φ_{type}	Φ: AN 0.76; HS 0.94; FT 0.99
Φ_{config}	Φ: Mono 0.78; Lami 0.75; Sym. IGU 0.96; Asym. IGU 1.10
$\Phi_{clearance}$	$\Phi_{clearance} = -0.17x + 2.87 \geq 1.0$ where *x* denotes glass-to-frame clearance (mm)
Φ_{system}	Φ: CW 1.0; SF 2.15
Φ_{aspect}	$\Phi_{aspect} = \begin{cases} if\ \ aspect\ ratio \leq 6:5, then: \Phi = \text{-}2.09\left(\frac{h}{b}\right) + 3.5 \\ if\ \ aspect\ ratio > 6:5, then: \Phi = 0.45\left(\frac{h}{b}\right) + 0.46 \end{cases}$ where *h* and *b* denote the height and width of a glass panel, respectively
$\Phi_{connection}$	1.0

Note: CW = Curtain wall; SF = Storefront

5. Final closed-form equation

5.1 Closed-form equation summary

The developed closed-form equation predicts the drift that causes cracking failure, while considering various glazing and configuration details of a glass system through the application of factors. Specifically, the equation takes into account the physical characteristics of glass-to-frame clearance and glass panel dimensions (accounted for within the ASCE equation), while additionally accounting for glass type (AN, HS, FT), glass configuration (Mono, Lami, sym. IGU, asym. IGU), glass system (CW or SF), and refining for substandard glass-to-frame clearances and a varying aspect ratio. Additionally, the equation allows for the future consideration of mullion-to-structure connection type. The final form of the equation is as defined in Eq. (24), and the definitions of all factors are summarized in Table 13.

5.2 Overall accuracy analysis

The accuracy of the final formulated closed-form equation is evaluated by comparing with the results of the ASCE equation and the experimental results. The percent difference of the predicted drift ratios of a given glass system based on Eq. (24) and those based on ASCE equation with respect to the experimental results provide a basis to assess the effectiveness of modification of ASCE equation to predict glass cracking drift capacity. The analysis and results are summarized in Table 14. A positive percentage in the last two columns indicates overestimation of the capacity, while a negative percentage means underestimation.

Overall, the average of the absolute percent differences decreases from 26.3% for the ASCE equation (Eq. 3) to 15.7% for the formulated equation (Eq. (24)). From these percentages, it can be concluded that the closed-form equation improves the accuracy of the predicted capacities of glass systems by a relative 40% compared to the ASCE equation. Moreover, the closed-form equation is more consistent in the degree of inaccuracy for prediction of glass cracking compared with the ASCE equation. This is illustrated by the high percent difference values of the ASCE equation, such as an overestimation of capacity by 93.7% for glass Configuration 1 compared to 14.8% by Eq. (24). This condition is illustrated in Fig. 12 where the percent differences from the last two columns of Table 14 are plotted for each glass configuration.

Finally, the cracking drift ratios obtained from experimental tests and the prediction equation (Eq. (24)) as listed in columns 8 and 9 as well as those predicted by ASCE equation (Eq. 3) are graphically compared for each glass configuration in Fig. 13. Referring to the plot, it can be seen how the ASCE predicted cracking drift ratios have been improved through the application of the factors in the form of the proposed equation relative to the experimental results. Glass configurations 3-5 as listed in Table 1 were combined into one data point and the same process was applied to glass Configurations 19 and 20 (with averages shown), since the configurations and results were relatively similar for these groups.

Overall, the plot illustrates that the predicted cracking drift ratios from the proposed equation more closely relfects the experimental cracking results and trends seen across the different glass configurations than those from the ASCE equation. For glass Configurations 1-6, which generally represent curtain wall systems with AN glass of varying glass panel configurations, the proposed

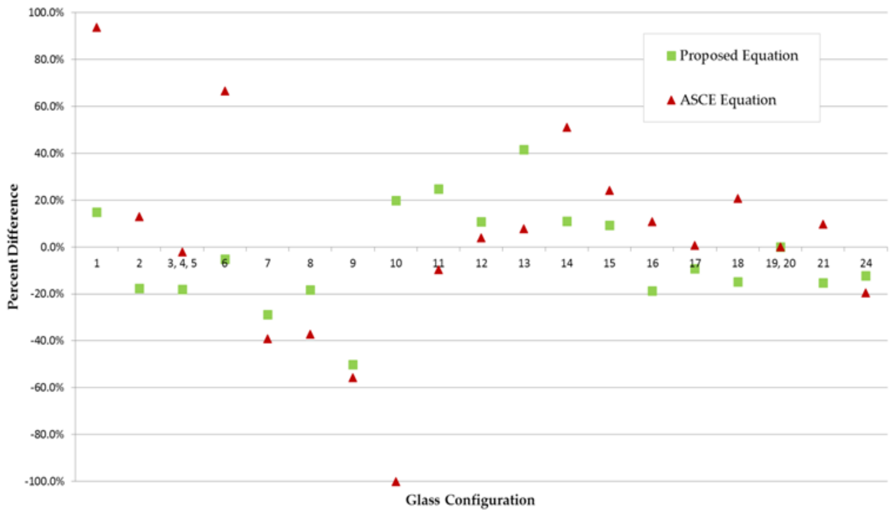

Fig. 12 Comparison of the percent differences between the proposed equation and the ASCE equation for each glass configuration listed in Table 1

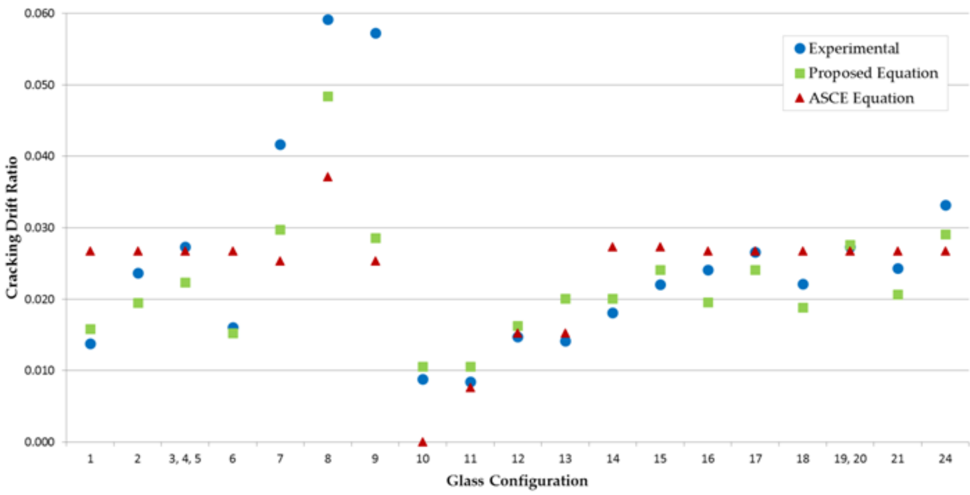

Fig. 13 Graphical comparison of predicted cracking drift ratio from the proposed equation, predicted cracking drift ratio from the ASCE equation, and experimental failure drift ratio for glass configurations

equation reflects the greater experimental capacities of the IGU Configurations 2-5 compared with the Mono and Lami Configurations of 1 and 6, respectively (while ASCE values are unchanged). Also, the proposed equation better reflects the increase in experimental cracking capacity of of storefront glass Configurations 7-9 compared with the ASCE equation. For glass Configurations 10-13 with substandard glass-to-frame clearances, the proposed equation eliminates the large cracking capacity inaccuracies. For glass Configurations 14 and 15 with varying glass panel aspect ratios, the plot shows that the proposed equation follows the trend seen with the experimental cracking as a result of varying aspect ratio. Finally, for glass Configurations 16-22 that represent

Table 14 Calculated percent difference between final closed-form equation, ASCE equation, and experimental cracking drift ratio values for all glass configurations

Config. ID	θ_{ASCE}	Φ_{type}	Φ_{config}	$\Phi_{clear.}$	$\Phi_{sys.}$	Φ_{aspect}	Cracking Failure (θ)		% Difference (Between Predicted and Experimental)	
							Pred. Eq. 24	Exp.	Pred. Eq. 24	ASCE Eq. 3
1	*2*	*3*	*4*	*5*	*6*	*7*	*8*	*9*	*10*	*11*
1	0.0267	0.76	0.78	1.0	1.0	1.0	0.0159	0.0138	14.8%	93.7%
2	0.0267	0.76	0.96	1.0	1.0	1.0	0.0195	0.0237	-17.6%	13.0%
3	0.0267	0.76	1.10	1.0	1.0	1.0	0.0224	0.0279	-19.9%	-4.2%
4	0.0267	0.76	1.10	1.0	1.0	1.0	0.0224	0.0270	-17.3%	-1.0%
5	0.0267	0.76	1.10	1.0	1.0	1.0	0.0224	0.0270	-17.3%	-1.0%
6	0.0267	0.76	0.75	1.0	1.0	1.0	0.0152	0.0161	-5.1%	66.5%
7	0.0253	0.76	0.78	1.17	2.15	1.0	0.0378	0.0417	-9.4%	-39.2%
8	0.0372	0.76	0.96	1.0	2.15	1.0	0.0583	0.0592	-1.6%	-37.2%
9	0.0253	0.76	0.75	1.17	2.15	1.0	0.0363	0.0573	-36.6%	-55.8%
10	0.0000	0.76	0.78	2.36	1.0	1.0	0.0107	0.0088	21.4%	-100.0%
11	0.0076	0.76	0.78	2.36	1.0	1.0	0.0107	0.0085	25.7%	-9.7%
12	0.0153	0.76	0.78	1.85	1.0	1.0	0.0168	0.0147	14.0%	3.9%
13	0.0153	0.76	0.96	1.85	1.0	1.0	0.0206	0.0142	45.2%	7.7%
14	0.0273	0.76	0.78	1.0	1.0	1.36	0.0201	0.0181	11.0%	51.1%
15	0.0273	0.76	0.78	1.0	1.0	2.46	0.0241	0.0220	9.4%	24.1%
16	0.0267	0.94	0.78	1.0	1.0	1.0	0.0196	0.0241	-18.8%	10.8%
17	0.0267	0.94	0.96	1.0	1.0	1.0	0.0241	0.0266	-9.2%	0.6%
18	0.0267	0.94	0.75	1.0	1.0	1.0	0.0188	0.0221	-14.9%	20.7%
19	0.0267	0.94	1.10	1.0	1.0	1.0	0.0276	0.0261	5.8%	2.3%
20	0.0267	0.94	1.10	1.0	1.0	1.0	0.0276	0.0285	-3.0%	-6.2%
21	0.0267	0.99	0.78	1.0	1.0	1.0	0.0206	0.0244	-15.2%	9.8%
22	0.0267	0.99	1.10	1.0	1.0	1.0	0.0291	0.0332	-12.3%	-19.5%
Average of Absolute Values[1]									15.7%	26.3%

[1]This value represents the average of the absolute percentage difference values

Table 15 Calculated factor values for example problem

Factor	Determined Values	
		Φ
	AN	0.76
Φ_{type}	HS	0.94
	FT	0.99
	$\Phi_{type} = 0.94$	

Table 15 Continued

Factor	Determined Values	
Φ_{config}		Φ
	Mono	0.78
	Lami	0.75
	Sym. IGU	0.96
	Asym. IGU	1.10
	$\Phi_{config} = \mathit{1.10}$	
Φclearance	$\Phi_{clearance} = -0.17(6) + 2.86 = \mathit{1.85}$	
Φsystem		Φ
	CW	1.0
	SF	2.15
	$\Phi_{system} = \mathit{1.0}$	
Φaspect	$\Phi_{aspect} = 0.45(2.4\text{ m} / 1.2\text{ m}) + 0.46 = \mathit{1.36}$	
Φconnection	*1.0*	

systems with HS and FT type glass, it can be seen that the predicted cracking values from the proposed equation generally follows the increases and decreases of the cracking experimental results for those systems (while ASCE equation is unchanged and mostly overestimates the cracking drift capacity).

A shortcoming of the proposed equation is that the degree of inaccuracy is slightly greater for glass Configurations 2-5, 11-13, 16, 17, 19, and 21 compared to the ASCE equation. This is a result of the ASCE equation predicting the capacity of certain glass configurations (a seemingly with less than 5% inaccuracy (while at the same time containing large inaccuracies for other configurations, such as 93.7% inaccuracy for Configuration 1). A majority of these configurations contained IGU's, which suggests that the ASCE equation happens to be most accurate for configurations with this glass configuration characteristic. Of course, the accuracy analysis has shown that, overall, the proposed equation is more accurate than the ASCE equation. Additionally, as a point of reference, for glass configurations where the ASCE equation is more accurate compared to the proposed equation, the degree of accuracy is 12.2% greater on average. For glassconfigurations where the proposed equation is more accurate compared to the ASCE equation, the degree of accuracy is 31.8% greater on average for the proposed equation. The accuracy of the proposed equation can also be improved as further testing is performed and the factor values are refined.

A concern regarding the proposed equation is that for select glass configurations the predicted capacity is not as accurate as ASCE while overestimating the capacity. This is the case for glass Configurations 10-13 with substandard clearances and glass Configuration 19 with an asymmetric HS IGU. It appears that for glass Configurations 10-13, the inaccuracy in the proposed equation is a result of limitations with the glass type factor values, specifically with the value for AN where overestimation is still present (overestimates by 14.8%, compared to 93.7% with ASCE equation). If this factor value is refined through further laboratory testing and becomes more accurate, then the predicted values for all glass configurations with AN glass (i.e., glass Configurations 10-13 with substandard clearances) will become more accurate as well. Also, for glass Configuration 13 (with the greatest inaccuracy), only one specimen of this configuration was tested. It is assumed that more testing of this glass configuration will yield a greater glass cracking experimental capacity, at which point the predicted cracking drift ratio from the proposed equation would become more accurate. The capacity for other glass configurations are also still overestimated, but significantly improved compared to the ASCE equation. For example, for glass configuration 1 the ASCE equation overestimates the capacity by 93.7%, while the proposed equation improves the accuracy but still overestimates by 14.8%. Overall, the proposed closed-form equation offers predicted cracking drift ratios that on the average better correspond to the experimental cracking results and trends across the varying glass configurations in Fig. 13.

5.3 Example

Assume a user desires to predict the drift that a proposed glass panel in a building can sustain before experiencing the glass cracking limit state. The glass panel is an 2.4 m high by 1.2 m wide asymmetric IGU, with an inner 6 mm AN-Mono pane, and an outer Lami unit with 6 mm HS lites in between a 1.5 mm PVB interlayer. The system utilizes a framing system comparable to the mid-rise curtain wall Kawneer 1600^{TM} framing system, and has a 6 mm glass-to-frame clearance.

The factor values are determined to input into the equation. The procedures and calculations used to find these values are seen in Table 15.

Using the identified factor values, the expected cracking capacity in terms of drift is found for the glass panel as follows:

$$\Delta_{crack} = (0.94)(1.1)(1.85)(1.0)(1.0)\left[2(6mm) + (1.36)\left(2(6mm)\left(\frac{2.4mm}{1.2mm}\right)\right)\right] = 85mm$$

The proposed closed-form estimates that the given configuration has a cracking drift capacity of 85 mm. In comparison, the ASCE equation estimates the cracking drift capacity of the same configuration to be 38 mm.

6. Summary and conclusions

The proposed closed-form equation developed to estimate the cracking failure drift of various glass curtain wall and storefront systems was formulated by using the ASCE 7-05 (same as ASCE 7-10) equation as its baseline with the application of various factors representing glazing characteristics that the ASCE equation does not consider. The ASCE equation was found to predict experimental glass cracking failure with a 26.3% inaccuracy on average. However, since the equation reasonably models the physical response of glass lites within a system subjected to seismic loads through the physical characteristics of glass-to-frame clearance and glass aspect ratio, it was used as the baseline in the formulation of the proposed equation.

Factors were developed based on trends extracted from the experimental data by isolating the various glazing variables that are known to affect glass capacity failure values. First, the Φ_{type} and Φ_{config} factors were created independently to account for glass type and configuration type, respectively. Then, $\Phi_{clearance}$, Φ_{system}, and Φ_{aspect} factors were developed to refine the prediction for the effect of clearances that are substandard, type of system, and glass panel aspect ratio, respectively. The magnitude of the effect of each of the factors typically varies from one glass configuration to another. However, in general, the predicted cracking drift is most sensitive to the parameters in the baseline equation, and, as a result, the physical characteristics of glass-to-frame clearance, height, and width dimensions of a glass panel still remain the primary characteristics, determining the expected glass cracking capacity.

Overall, the proposed equation with applied factors as defined in Table 13 is relatively easy to use. For the baseline equation (Eq. 3), only glass-to-frame clearance and panel dimensions need to be input. For the values of the Φ_{type}, Φ_{config}, and Φ_{system} factors, a user only has to select the appropriate factor value from a discrete set of values. For the $\Phi_{clearance}$ and Φ_{aspect} factors, if the clearance or aspect ratio is not standard, the corresponding dimensions are input into the factor definition to produce a factor value. Since the calculations can be performed using a standard calculator, the proposed closed-form equation it is relatively simple to use.

The proposed closed-form equation has been shown to improve the accuracy of predicting the cracking capacity of glass systems as compared to the ASCE equation, and, therefore, has the potential to be a useful architectural glass design tool for professionals. In the overall comparison, the proposed closed-form equation was shown to reduce the percent difference between the experimental and predicted values from 26.3% from the ASCE equation to 15.7%. Also, a comparison between the percent differences of the proposed and ASCE equations showed that the proposed equation is more consistent and eliminates large inaccuracies for any given glass configuration.

The proposed closed-form equation has applications for a broad range of curtain wall and storefront systems. Follow-up studies and analysis on available data can also extend the reach of the equation to glass systems with other glazing characteristics. Specifically, it would be desired to modify the equation so that it considers wet-glazed structural silicone glazing systems, unitized systems, and the effects of other commonly employed mullions-to-structure connections. Additionally, further studies on modern storefront configurations, glass configurations with glass-to-frame clearances greater than 11 mm, configurations with other aspect ratios not considered in this paper, and curtain wall or storefront systems with corner conditions could be used to further refine the factor definitions and values.

Acknowledgements

The support of manufacturers such as Kawneer and Oldcastle Glass that have provided material for testing over the years is gratefully acknowledged. The support of Dr. Richard Behr and Paul Kremer whom provided guidance with this research is acknowledged. The opinions, results and conclusions expressed in this paper are only those of the authors and do not necessarily represent the views of any of the sponsors.

References

American Architectural Manufacturers Association (AAMA), (2009), *Recommended Dynamic Test Method for Determining the Seismic Drift Causing Glass Fallout from a Wall System*, Publication No. AAMA 501.6-09.

American Society of Civil Engineers (ASCE), (2006), *Minimum Design Loads for Buildings and other Structures*, ASCE 7-06, ASCE, Reston, VA.

American Society of Civil Engineers (ASCE), (2010), *Minimum Design Loads for Buildings and other Structures*, ASCE 7-10, ASCE, Reston, VA.

Behr, R.A., Belarbi, A. and Brown, A.T. (1995), "Seismic performance of architectural glass in a storefront wall system", *Earthq. Spectra*, **11**(3), 367-391.

Behr, R.A. and Belarbi, A. (1996), "Seismic test methods for architectural glazing systems", *Earthq. Spectra*, **12**(1), 129-143.

Behr, R.A. (1998), "Seismic performance of architectural glass in mid-rise curtain wall", *J. Architect. Eng.*, **4**(3), 94-98.

Bouwkamp, J.G. and Meehan, J.F. (1960), "Drift limitations imposed by glass", *Proceedings of Second World Conference on Earthquake Engineering*, Tokyo, Japan, 1763-1778.

Bouwkamp, J.G. (1961), "Behavior of window panel under in-plane forces", *Bull. Seismol. Soc. Am.*, **51**(1), 85-109.

Bull, E. and Cholasky, J. (2012), "A review of the behavior of structural silicone glazing systems subjected to a mega-earthquake", *ASTM Int.*, **9**(5), May 2012, DOI: 10.1520/JAI104151, 25p.

EERI, (1995), *Northridge Earthquake Reconnaissance Report*, **1**, *Earthquake Spectra*, Supplement to Volume 11, Earthquake Engineering Research Institute, Oakland, California.

Eva, C. and Hutchinson, T.C. (2011), "Experimental evaluation of the In-Plane seismic behavior of storefront window systems", *Earthq. Spectra*, **27**(4), November 2011, 997-1021.

Gasparella, A., Pernigotto, G., Cappelletti, F., Romagnoni, P. and Baggio, P. (2011), "Analysis and modelling of window and glazing systems energy performance for a well insulated residential building," *Energy Buildi.*, **43**(4), April 2011, 1030-1037.

Hutchinson, T.C., Zhang, J. and Eva, C. (2011), "Development of a drift protocol for seismic performance evaluation considering a damage index concept", *Earthq. Spectra*, **27**(4), 1049-1076.

Hamburger, R. (2006), The ATC-58 Project: Development of Next-Generation Performance-Based Earthquake Engineering Design Criteria for Buildings, Structures Congress 2006: pp. 1-8.
doi: 10.1061/40889(201)31.

International Code Council (ICC), (2006), *International Building Code (IBC) 2006*, ICC, Falls Church, VA.

Kim, K.H. (2011), "A comparative life cycle assessment of a transparent composite façade system and a glass curtain wall system", *Energy Build.*, **43**(12), December 2011, 3436-3445.

Lee, E., Selkowitz, S., Bazjanac, V., Inkarojrit, V. and Kohler, C. (2002), *High-Performance Commercial Building Facades*, Lawrence Berkeley National laboratory, eScholarship, University of California, http://escholarship.org/uc/item/7d30b3rd, June 2002, 133 p.

Memari, A.M., Behr, R.A. and Kremer, P.A. (2003), "Seismic behavior of curtain walls containing insulating glass units", *J. Architect. Eng.*, ASCE, **9**(2), 70-85.

Memari, A.M. (editor), (2013), *Curtain Wall Systems: A Primer*, *ASCE Manuals and Reports on Engineering Practice No. 126*, American Society of Civil Engineers, Reston, VA, 2013, 217.

Memari, A.M. (2012), "Review of the performance of glazing systems in earthquakes and recent developments to mitigate damage", *Proceedings of the ASCE 6th Congress on Forensic Engineering – Gateway to a Safer Tomorrow*, San Francisco, CA October 31-November 3, 123-132.

National Institute of Building Sciences (NIBS) (2008), *Whole Building Design Guide*, www.wbdg.org, prepared by the National Institute of Building Sciences, July 15.

O'Brien, W.C., Memari, A.M., Kremer, P.A. and Behr, R.A. (2012), "Fragility curves for architectural glass in stick-built glazing systems", *Earthq. Spectra*, **2**(28), 639-665.

Richman, R.C. and Pressnail, K.D. (2009), "A more sustainable curtain wall system: Analytical modeling of the solar dynamic buffer zone (SDBZ) curtain wall", *Build. Environ.*, **44**(1), January 2009, 1-10.

Whole Building Design Guide (WBDG) (2009), www.wbdg.org.

Sucuoglu, H. and Vallabhan, C.V.G. (1997), "Behavior of window glass panels during earthquakes", *Eng. Struct.*, **19**(8), 685-694.

CC